

# Simulation of Ultra-Fast Dynamics Effects in Resonant Inelastic X-Ray Scattering of Gas Phase Water

Adam E. A. Fouda, Gregory I. Purnell and Nicholas A. Besley\*

*School of Chemistry, University of Nottingham, University Park, Nottingham, NG7 2RD, UK.*

E-mail: [nick.besley@nottingham.ac.uk](mailto:nick.besley@nottingham.ac.uk)

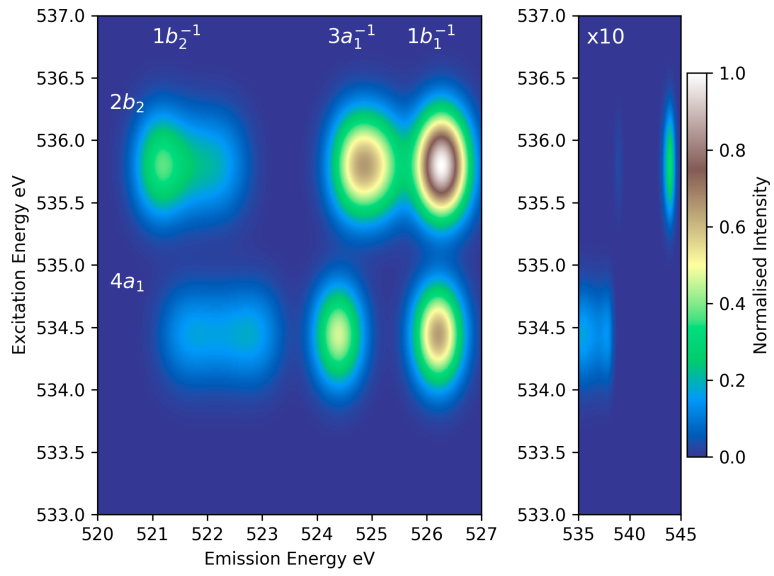
## Abstract

Resonant inelastic soft x-ray scattering maps for the water molecule are simulated by combining quantum chemical calculations of x-ray spectroscopy with *ab initio* molecular dynamics. The resonant inelastic scattering intensity is computed using the Kramers-Heisenberg formalism which accounts for channel interference and polarisation anisotropy. Algebraic diagrammatic construction and density functional theory based approaches for the calculation of the x-ray transition energies and transition dipole moments of the absorption and emission processes are explored. Conformational sampling of both ground and core-excited intermediate states allows the effects of ultra-fast dynamics on the computed maps to be studied. Overall, it is shown how resonant inelastic scattering maps can be simulated with a computationally efficient protocol that can be extended to investigate larger systems.

---

\*To whom correspondence should be addressed

## Table of Contents Graphic



## Introduction

The ongoing development of synchrotron and free-electron laser sources has led to continued advances in spectroscopic techniques using x-rays. The use of x-rays as effective structural probes and their applicability to study ultrafast chemical processes underpins a growth in both experimental and theoretical research.<sup>1-5</sup> One fast developing technique is resonant inelastic x-ray scattering (RIXS),<sup>6</sup> which is a two step procedure wherein the initial state of the system is excited to an intermediate core-excited state and emission from this state leads to the final state. For direct scattering, RIXS can be viewed as synonymous with resonant x-ray emission (RXES). RIXS combines the element specific nature of x-ray spectroscopic techniques with the flexibility to probe different intermediate states, and furthermore, RIXS is not limited by the optical selection rules.

Recently, RIXS studies have been reported for a range of molecules.<sup>7-12</sup> The focus of this paper is the water molecule. X-ray absorption and x-ray emission studies have played a central role in an on-going debate regarding the structure of liquid water,<sup>13-15</sup> which has led to the concept of high density and low density water structures.<sup>16-18</sup> The first non-resonant XES study of gas phase water was reported by Guo *et al.*<sup>19</sup> More recently, gas phase RIXS spectra of H<sub>2</sub>O and D<sub>2</sub>O were measured with a higher signal to noise ratio and covering a range of intermediate states. Shifts in energy, variation in the relative intensities of the emission lines for different intermediate states and new features associated with dissociated H<sub>2</sub>O were observed.<sup>8</sup> RIXS studies have also shown that control and selection of vibrational excitation can be achieved by selectively tuning core-excited molecular bands.<sup>20,21</sup> Gas-phase water often serves as a precursor to examining liquid water and a number of studies have investigated the RIXS of liquid water.<sup>19,22-26</sup>

Computational simulations can play an important role in understanding and interpreting RIXS spectra measured in experiment. Quantum chemical methods are routinely used to simulate x-ray absorption and emission spectra. For example, x-ray absorption spectra can be computed using static-exchange, transition potential and Bethe-Salpeter methods.<sup>27-32</sup> X-ray absorption spectra

can also be computed using time-dependent density functional theory (TDDFT)<sup>33–39</sup> as well as wavefunction based methods that include electron correlation.<sup>40–43</sup> It has been shown that accurate non-resonant x-ray emission spectra can be simulated within the framework of equation of motion coupled cluster theory including single and double excitations (EOM-CCSD) and TDDFT by using a reference determinant that describes the core-ionised state. These approaches have been used to study water clusters<sup>44</sup> and organic and inorganic systems,<sup>45–47</sup> and recently the x-ray emission spectroscopy of liquid water.<sup>48</sup> More simply, x-ray emission spectra can be determined directly from a Kohn-Sham DFT calculation, where the transition energy is evaluated as the difference between the orbital energies of the valence and core orbitals, and the associated intensity can be determined from the transition matrix element between the initial and final states  $f \propto |\langle \phi_c | \hat{\mu} | \phi_v \rangle|^2$ . Here a valence orbital ( $\phi_v$ ) is taken to be the initial state and the final state is a core orbital ( $\phi_c$ ). Recently, it has been shown that this approach can provide accurate x-ray emission spectra when the DFT calculation is performed with a short-range corrected exchange-correlation functional.<sup>49,50</sup> This approach was extended to simulate RXES in a two-step procedure where a reference determinant describing the intermediate core-excited state is used in the Kohn-Sham DFT calculation. It was necessary to average over a number of structures from a molecular dynamics simulation in the core-excited state to achieve agreement with experiment.

In comparison to calculations of x-ray absorption and emission spectra, the application of quantum chemical based methods to simulate RIXS is considerably less well developed. RIXS can be simulated based upon the formalism of Kramers and Heisenberg who introduced electronic coherence effects between two photon transitions in atomic systems.<sup>51</sup> Their formalism was later developed by Gel'mukhanov and co-workers,<sup>52–54</sup> who incorporated consideration of the polarisation anisotropy and channel interference between the excitation and resonant emission processes. The interaction between the linearly polarised incident photon, the orientation of the molecule and the transition dipole moments between the core electron excitation and the subsequent collapse of the valence electrons to the core all result in an angular dependence of the intensity of

resonant emission and the overall RIXS cross-section. An overview of this approach is available elsewhere.<sup>55</sup>

Calculations of the RXES of liquid water have been reported.<sup>24,56</sup> These studies use small water clusters to represent different hydrogen bonding environments present in liquid water. The intensities of the bands in the emission spectra were determined using a group theory formalism<sup>56</sup> and from the  $p$  orbital population of the excited atom.<sup>24</sup> It has been established that vibrational interference effects can play an important role in x-ray emission spectroscopy,<sup>57,58</sup> The Kramers-Heisenberg formalism has been used to describe vibrational interference effects in the x-ray emission spectrum of the water dimer, and this work is summarised in the review by Nilsson *et al.*<sup>59</sup> The intermediate state representation (ISR) within ADC<sup>60</sup> provides a framework for describing excited states and determining excited state properties.<sup>61</sup> Very recently, Rehn *et al.*<sup>62</sup> developed a ADC/ISR scheme to provide a first principles description of inelastic scattering through the integration of complex polarisation propagator theory into the Kramers-Heisenberg (KH) equation. Determining RIXS 'maps' reported in experimental studies<sup>8</sup> presents several challenges to quantum chemical based calculations. It is necessary to have a reliable description of the both the excitation and emission processes, the resulting RIXS cross-sections need to be determined via (for example) the KH equation and these intensities need to be combined to give a resulting map. A further complicating factor is that consideration of nuclear dynamics can be important, and the dynamics of the core-excited intermediate state may differ significantly from the ground state. Ideally this should be achieved using approaches that can be applied to relatively large systems. A semiclassical approximation to the KH equation has been introduced for the modelling of core-hole induced dynamics.<sup>63</sup> In this approach the initial conditions are sampled from the quantum zero-point position and momentum distributions of the OH vibration and it has been applied to study liquid methanol and ethanol,<sup>64,65</sup> in addition to water.<sup>63</sup> Recently, this approach has been extended to consider resonant x-ray emission.<sup>66</sup>

In this study, we simulate the RIXS spectrum of a water molecule using an approach that explicitly considers the intermediate state. The vibrational degrees of freedom are sampled by averaging over structures derived from *ab initio* molecular dynamics (AIMD) simulations<sup>67</sup> for both the ground and intermediate states and the use of both wavefunction and DFT based methods to describe the absorption and emission processes is explored.

## Method and Computational Details

An overview of the different steps in determining the RIXS maps are as follows, with further details of the calculations described subsequently

1. AIMD simulations are performed for the ground and core-excited states and the structures sampled from each simulation.
2. The absorption and emission energies and associated transition dipole moments are determined using electronic structure calculations.
3. The RIXS intensities for the different absorption and emission energies are determined from the KH equation.
4. Normalised spectra for each structure are fitted to independent 2-dimensional Gaussian functions and summed and renormalised to produce a RIXS map.

### *Ab Initio* Molecular Dynamics Simulations

AIMD calculations were performed using DFT with the B3LYP exchange-correlation functional and aug-cc-pCVTZ basis set. The inclusion of core-valence correlation functions in the basis set has been shown to be important for describing core-excited states.<sup>68</sup> The purpose of these simulations is to provide representative structures for the ground and core-excited states. Simulations were performed for the ground state and  $4a_1$  and  $2b_2$  core-excited states. It is known that the  $4a_1$  undergoes ultra-fast dissociation, as a consequence of this and the lifetime of the core-excited state

being approximately 3.6 fs, a short simulation time of 3.8 fs is used for  $4a_1$  and  $2b_2$  core-excited state simulations. In practice, the life-time of the intermediate state is not fixed and is represented by an exponential decay. Consequently, it is possible for the intermediate state to have a longer lifetime than the typical 3.6 fs. Furthermore, it is also possible for the water molecule to dissociate on a faster time scale depending on the initial conditions. When comparing the computed spectra with experiment (see later) we also consider the presence of fully dissociated  $H^+—OH^-$ . The water molecule represents an example of where the nuclear dynamics of the intermediate state are very different from the ground state, making explicit consideration of the molecular dynamics of the core-excited intermediate state necessary. The core-excited state simulations were run using the maximum overlap method (MOM)<sup>69</sup> to prevent variational collapse. MOM calculations start with an initial guess formed by removing one selected core orbital from the spin-beta space of the converged neutral orbitals, and then preserves the excited hole state from collapsing by maintaining maximum overlap of orbitals between successive iterations of the self-consistent field (SCF) procedure. In the application of MOM to study core-excited states it can be useful to consider the overlap with the initial guess, rather than the previous iteration of the SCF calculation.<sup>70</sup> Ground state dynamics were run for a longer simulation period of 13.2 fs, capturing the full extent of the ground state conformations. All simulations were initiated with thermally derived velocities using a temperature of 383 K, consistent with the experimental conditions.<sup>8</sup> It has been shown that for dissociative states large zero-point energy in the OH stretch can have a significant influence on the resulting dynamics.<sup>63</sup> However, in this study we do not explicitly consider sampling of the initial conditions from the quantum distributions. For the DFT calculations, 40 structures were sampled at equally spaced time intervals from each simulation. The different simulation times for the core-excited and ground state dynamics results in time-steps of 0.096 fs and 0.24 fs, for the core-excited and ground state simulations, respectively. For the ADC calculations, only 10 structures were sampled for each simulation owing to the comparatively high cost of ADC calculations. To maximise the extent of conformational sampling and the channel interference between initial and final states, each individual ground state structure was linked to each core excited state struc-

ture through the KH equation for both core-excited states. This results in 3200 spectra of unique coordinate combinations for the DFT calculations.

## Electronic Structure Calculations

Electronic structure calculations were performed based upon the ADC and DFT methods using the aug-cc-pCVTZ basis set. Within the framework of the ADC method, core-excited states can be determined using the core-valance separation (CVS) approach where the coupling between the valance and core is assumed to be zero. Further details of this method have been reported.<sup>43,71</sup> Core-excited states were determined for the ground state structures using the extended second order CVS-ADC (CVS-ADC(2)-x) method as recommended by Neville *et al.*<sup>72</sup> The ground state wavefunction of ADC(2) is calculated by second order Møller-Plesset perturbation theory (MP2). In the approach used here, the resonant emission energies and their associated transition dipole moments were calculated by performing ADC(2)-x on a core excited wavefunction generated by using MOM and MP2. The CVS approximation is not required because the relevant transition energies are negative.

For the DFT calculations, x-ray absorption energies and transition dipole moments were determined for the ground state structures using TDDFT within the Tamm-Dancoff approximation (TDA).<sup>73</sup> The SRC1-R1 exchange-correlation functional<sup>74</sup> was used, this functional has been shown to be accurate for core-excited states for a range of systems.<sup>38,75-77</sup> Two different approaches were investigated for the calculation of the emission spectra for the different intermediate states. In the first approach, the emission energies and transition dipole moments are determined directly from the Kohn-Sham DFT calculation using the following

$$\Delta E = \varepsilon_v - \varepsilon_c . \quad (1)$$

The associated intensity can be determined from the transition matrix element between the initial

and final states

$$f \propto |\langle \phi_c | \hat{\mu} | \phi_v \rangle|^2 \quad (2)$$

where a valence orbital ( $\phi_v$ ) is taken to be the initial state and the final state is a core orbital ( $\phi_c$ ). It has also been shown that this method gives good agreement with experiment for RIXS spectra when used in conjunction with the B3LYP functional.<sup>49</sup> In addition, the emission spectra were determined using TDDFT with the TDA and B3LYP functional. In these calculations the relevant core-excited determinant is used as the reference for the TDDFT calculation. All electronic structure calculations were performed using the QCHEM software package.<sup>78</sup> The calculations do not include relativistic effects. For the oxygen K-edge it is common to include a correction of +0.3 eV to account for relativistic effects.<sup>79</sup> This correction has been included in the calculated energies and the one dimensional spectra compared with experiment.

### Kramers-Heisenberg Equation

The RIXS intensities can be determined from the transition energies and transition dipole moments of the excitation and emission processes using the KH equation. Here we follow the formalism presented by Gel'mukhanov and co-workers which accounts for channel interference and polarisation anisotropy effects.<sup>62</sup> The unpolarised intensity  $I_o$  can be derived from the channel interference between scattering channels,

$$I_o \propto \sum_k \zeta_{vn}^{k*} \zeta_{vn}^k, \quad (3)$$

where

$$\zeta_{vn}^k = \frac{\alpha \omega_{vk} \omega_{nk}(\mathbf{v})}{\omega' - \omega_{nk} + i\Gamma} d_{vk} d_{nk}. \quad (4)$$

The index  $k$  refers to the core orbital, and the labels  $v$  and  $n$  refer to the virtual orbital the core electron is excited to and the occupied orbital an electron collapses to, respectively.  $\alpha$  is equal to

$137^{-1}$  and  $\Gamma$  is the broadening associated with the lifetime of the core-excited state and has a value of 0.1 eV.<sup>80</sup> This term is assumed to be constant and not dependent on the nuclear coordinates<sup>81</sup> and it determines the amount of interference between different intermediate channels<sup>58</sup> and provides a limit to the resolution of the spectra.  $\omega_{vk}$  and  $d_{vk}$  are the transition energy and transition dipole moment for the core $\rightarrow$ virtual orbital excitation, while  $\omega_{nk}(\nu)$  and  $d_{nk}$  are the transition energy and transition dipole moment for the occupied $\rightarrow$ core orbital transition. The emission energy is dependent on the nature of the intermediate state since there will be variation in screening effects between the different states.<sup>82</sup>  $\omega'$  is the energy of the emitted photon, for simple single core orbital molecules such as water, this will equal  $\omega_{nk}$ . However in more complex systems with increased scattering channels this will not necessarily be the case. The intensity can be expressed as a function of the angle between the polarization vector of the linearly polarised incident beam and the propagation direction of the outgoing photon ( $\theta$ ). In this work  $\theta$  is set 45 degrees to be consistent with experimental conditions.<sup>8</sup>

The perpendicular and parallel ( $I_{\perp}(\theta)$  and  $I_{\parallel}(\theta)$ ) components of the intensity can be determined using the anisotropy parameter R,

$$I(\theta) = I_{\perp}(\theta) + I_{\parallel}(\theta), \quad (5)$$

where

$$I_{\perp}(\theta) = \frac{1}{2}I_o[1 - R], \quad (6)$$

$$I_{\parallel}(\theta) = \frac{1}{2}I_o[1 + R(3 \sin^2 \theta - 1)] \quad (7)$$

and

$$R = \frac{1}{5}(3 \cos^2 \phi - 1). \quad (8)$$

$\phi$  is the angle between absorption and emission dipole moments. Since the water has only one core orbital there is no core channel scattering which simplifies the formalism, as detailed in reference.<sup>62</sup>

## Map Generation

RIXS maps are formed by fitting 2D gaussian functions to the individual peaks of a normalised spectrum. 1600 RIXS maps containing both  $4a_1$  and  $2b_2$  core-excited intermediate states are generated from the structures sampled from the AIMD simulations. The gaussian functions are summed on a grid and then the final grid is renormalised. Gaussian broadening of 0.25 eV and 0.30 eV was applied to the excitation and emission energy coordinates respectively in the maps. All 1D spectra presented in this study were broadened by 0.20 eV.

## Results and Discussion

The structural changes that occur during the AIMD simulations have a critical role in the appearance of the simulated RIXS spectra. The lifetime of the core-excited states is of the order of femtoseconds enabling the ultra-fast dissociation phenomena often attributed to core-excited states to be probed. The dissociation of the water molecule in the  $4a_1$  core-excited state has been observed in x-ray fragment diffraction and Auger spectroscopy studies.<sup>83,84</sup> The length of the AIMD simulations for the core-excited states is 3.8 fs which reflects the lifetime of this state, and Table 1 summarises the changes in the O-H bond lengths that occur during the AIMD simulations for the  $4a_1$  and  $2b_2$  core-excited states. For both core-excited states the O-H bond lengths increase during the simulations. In the  $4a_1$  intermediate state the lengthening of the bonds is asymmetric with one bond stretching more. This represents the early stages of dissociation and for longer simulations dissociation is observed. We note that the AIMD simulations performed will not account for non-adiabatic effects and hence an accurate estimation of the core-lifetime is not to be expected. In

contrast to for  $4a_1$ , the  $2b_2$  state has a more symmetric extension of the bonds. The RIXS spectra that result from sampling the structures from these dynamics simulations will reflect the changing symmetry of the water molecule that occurs during the relaxation in the intermediate state.

Table 1: Maximum bond lengths for the  $4a_1$  and  $2b_2$  core-excited states during a 3.8 fs B3LYP/aug-cc-pCVTZ AIMD simulation and their deviation from the initial equilibrium ground state structure ( $r_{OH}=0.962 \text{ \AA}$ ).

State	Bond	$r_{max} / \text{\AA}$	$\Delta r / \text{\AA}$
$4a_1$	$r_{OH1}$	1.055	0.094
	$r_{OH2}$	1.170	0.208
$2b_2$	$r_{OH1}$	1.159	0.194
	$r_{OH2}$	1.158	0.196

Detailed analysis of the x-ray absorption and x-ray emission spectra of water are reported elsewhere.<sup>24,56</sup> In the water molecule, the three highest occupied valence orbitals are the  $1b_2$ ,  $3a_1$  and  $1b_1$  orbitals, while the two lowest unoccupied orbitals are the  $4a_1$  and  $2b_2$  orbitals. The RIXS spectrum measured in experiment<sup>8</sup> considers the two higher energy  $2b_1$  and  $5a_1$  in addition to the  $4a_1$  and  $2b_2$  states. In our calculations, the MOM procedure is unable to describe the  $5a_1$  state, and in this study we focus on the lower energy  $4a_1$  and  $2b_2$  intermediate states. The calculation of higher lying states is problematic for this approach, however, progress in overcoming these limitations is being made.<sup>85</sup> Table 2 shows the core-excitation energies calculated at the equilibrium ground state structure for CVS-ADC(2)-x and TDDFT methods. The CVS-ADC(2)-x values underestimate the experimental values by 1.0 eV however, this underestimation is consistent for the two states. Consequently, the energy difference between the two states is predicted correctly. An advantage of DFT based calculations is that they can be more readily applied to study larger systems, owing to their lower computational cost. TDDFT excitation energies have been computed with the SRC1-R1 exchange-exchange correlation functional.<sup>74</sup> This functional is designed for the calculation of core-excitation energies and the calculated excitation energies are closer to experiment. Although, the separation between the two states is predicted less accurately.

Table 2: Calculated and experimental XAS transition energies (in eV) with the errors with respect to experiment<sup>86</sup> given in parentheses, including a correction of +0.3 eV for relativistic effects.<sup>79</sup>

State	Exp.	CVS-ADC(2)-x	TDDFT: SRC1-R1
4a <sub>1</sub> (1s→4a <sub>1</sub> )	534.0	533.0 (-1.0)	534.8 (+0.8)
2b <sub>2</sub> (1s→2b <sub>2</sub> )	535.9	534.9 (-1.0)	536.1 (+0.2)

Table 3: Calculated and experimental RXES transition energies (in eV), including a correction of +0.3 eV for relativistic effects.,<sup>79</sup> with the errors with respect to experiment<sup>8</sup> given in parentheses. TDDFT emission energies have been shifted by -9 eV.

Intermediate State	Emission Line	Exp.	ADC(2)-x	KS-DFT	TDDFT
4a <sub>1</sub>	1b <sub>1</sub>	526.6	526.2 (-0.4)	526.4 (-0.2)	526.2 (-0.4)
	3a <sub>1</sub>	524.2	523.9 (-0.3)	524.6 (+0.4)	524.0 (-0.2)
	1b <sub>2</sub>	522.1	520.1 (-2.0)	521.6 (-0.5)	522.3 (+0.2)
2b <sub>2</sub>	1b <sub>1</sub>	526.8	526.2 (-0.6)	526.5 (-0.3)	526.4 (-0.4)
	3a <sub>1</sub>	524.6	523.9 (-0.7)	524.9 (+0.3)	524.5 (-0.1)
	1b <sub>2</sub>	520.8	520.2 (-0.6)	521.4 (+0.6)	522.1 (+1.3)

The resonant x-ray emission energies for the two intermediate states are shown in Table 3. The ADC(2)-x method tends to underestimate the size of the transition energies. The separation between the different transitions is predicted accurately with the exception of the 1b<sub>2</sub> emission line for the 4a<sub>1</sub> intermediate state. However, as shown later, this state is significantly affected when the dynamics of the intermediate state are taken into account. The KS-DFT values calculated with the B3LYP exchange-correlation functional are in good agreement with the experimental values. This is the computationally least expensive of the three methods and has the potential to be applied to study much larger systems. The transition energies computed with TDDFT are too high owing to self interaction error in DFT,<sup>45,87</sup> and a shift of -9 eV has been applied to the transition energies shown. Once this shift is applied, the TDDFT calculations provide a good description of the emission energies.

The structures extracted from the AIMD simulations have C<sub>s</sub> symmetry, and the orbitals of a<sub>1</sub>

and  $b_1$  symmetry will have  $a'$  symmetry and  $b_2$  orbitals will be  $a''$ . However, in the calculated RIXS maps we retain the  $C_{2v}$  point group labels. The evolving nature of the molecular orbitals and associated transition dipole moments during the molecular dynamics simulations will be reflected in the channel interference and the polarisation anisotropy effects of resonant emission. These effects are important for an accurate description of the RIXS intensity and are described by the KH equation. In a RIXS experiment of a gas-phase sample, the molecules will have random orientation and the incident x-ray beam is linearly polarised by the undulator source with the detector positioned at a fixed angle from the polarisation vector (45 degrees in this case<sup>8</sup>). The probability of excitation will depend on the relationship between the polarisation vector and the transition dipole moment between the core and unoccupied valence excited state. Furthermore, the intensity of the emission will be dependant on the symmetry of the intermediate state.

The simulated RIXS spectral maps based upon ADC, DFT and TDDFT methods are shown in Figures 1-3. For each method, maps are presented based upon the single equilibrium structure and when averaging over conformation is included. This allows the effect of nuclear dynamics and the different computational methodologies to be assessed. In the computed RIXS maps, the intensity is color-coded as a function of absorption and emission intensities and can be compared directly with the experimental data reported previously.<sup>8</sup> There are a number of features observed in experiment that can be used to assess the accuracy of the computational simulations. For the  $3a_1^{-1}$  and  $1b_1^{-1}$  states there is a shift to higher energy with increasing excitation energy, while the  $1b_2^{-1}$  emission band only has a small shift. This is referred to as the spectator shift and arises from screening effects and from the angular isotropy of the emission process.<sup>82</sup> The most intense peak in the map is the  $1b_1^{-1}$  band for the  $2b_2$  intermediate state. A further feature of the maps is the evidence of nuclear dynamics, with additional features visible for the  $4a_1$  state. These features were associated with OH fragments formed following dissociation in the intermediate state.

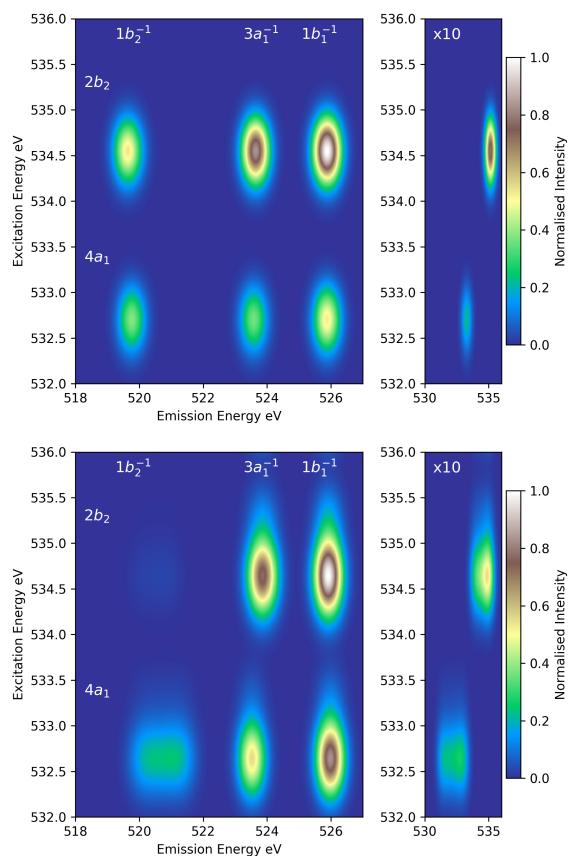


Figure 1: Simulated RIXS maps of gas phase water calculated with ADC methods for the equilibrium water structure (top) and sampling structures attained from AIMD simulations (bottom). Left panels shows the inelastic region (spectator emission) and the right panel shows the elastic scattering peaks (participant emission).

The ADC RIXS map for a single conformer shows peaks at approximately the correct energies, although the absorption energies are underestimated a little, and correctly predicts the  $1b_1^{-1}$  peak for the  $2b_2$  intermediate state to be the most intense. However, there is little evidence of spectator shifts. The elastic scattering peaks (participant electron emission) are also described well in terms of their energies and relative intensities. On the inclusion of molecular dynamics some noticeable changes become evident. These are most significant for the  $1b_2^{-1}$  emission, where there is a loss of intensity for the  $2b_2$  intermediate state and a large degree of broadening of the emission energy for the  $4a_1$  intermediate state. Similar broadening is also observed for the elastic scattering lines.

There is a small spectator shift in the energy of the  $3a_1$  emission band but not for the  $1b_1^{-1}$  band.

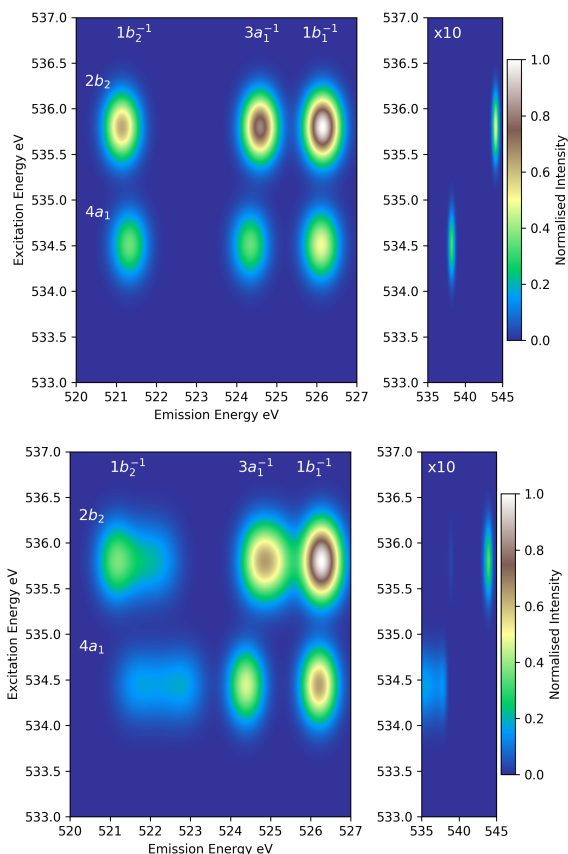


Figure 2: Simulated RIXS maps of gas phase water calculated with TDDFT for the absorption and Kohn-Sham DFT for the emission for the equilibrium water structure (top) and sampling structures attained from AIMD simulations (bottom). Left panels shows the inelastic region (spectator emission) and the right panel shows the elastic scattering peaks (participant emission)

For the ADC simulations if the RIXS maps only a limited amount of conformational averaging was performed. For the computationally less demanding DFT methods, more extensive sampling can be used more readily. Consequently, it is informative to establish how these methods perform for the simulation of RIXS maps. Figure 2 shows the RIXS map generated using TDDFT to describe the absorption process and the properties of the emission determined directly from the Kohn-Sham DFT calculation. The map for a single conformation shows that this approach pro-

vides a qualitatively correct description. The absorption and emission energies for the spectral bands are consistent with experiment, and the correct peak is identified as the most intense. The largest discrepancy for this method is the energies of the elastic peaks, which are too high. On the inclusion of conformational sampling the peaks are broadened significantly, particularly in the  $4a_1$  emission line, and spectator shifts are observed for the  $3a_1^{-1}$  and  $1b_1^{-1}$  bands. A key observation is that the effects of ultra-fast dissociative are evident in the simulations for the  $4a_1$  intermediate state. In the AIMD simulation for the  $4a_1$  intermediate state the water molecule is not fully dissociated. The experimental spectrum shows distinct features associated with  $\text{OH}^-$  arising from a fully dissociated water molecule. We will return to discuss these features later. One potential improvement in the simulation protocol would involve multiple AIMD simulations for the core-excited states, each started at different ground state conformations. Such an approach has been used in AIMD investigations combined with Auger spectroscopy,<sup>88</sup> but would result in a significant increase in computational cost. A more complete sampling of initial conditions has also other studies.<sup>63</sup> Other avenues for improvements would be the use of high level quantum nuclear dynamical methods such as the variational multi-configurational Gaussian (vMCG) method.<sup>89</sup>

Using TDDFT to describe the emission process also provides a good description of the RIXS maps, with the relative energies and intensities of the peaks predicted accurately (see Figure 3). However, the computed energies are systematically too high, which is associated with the self-interaction error present with the B3LYP exchange-correlation functional.<sup>45</sup> However, this error is systematic and applying a constant shift to the emission energies of about -9 eV brings the map into alignment with the experiment. An advantage of the TDDFT approach is that the relative energies of the elastic scattering peaks relative to the spectator peaks is predicted correctly.

Figure 4 illustrates the variation of the resonant x-ray emission spectra along core-excited trajectories for the  $4a_1$  and  $2b_2$  core-excited states. The spectra for the dynamics (blue curves) along with the spectra for the ground state equilibrium starting structure (red curve). This shows how the

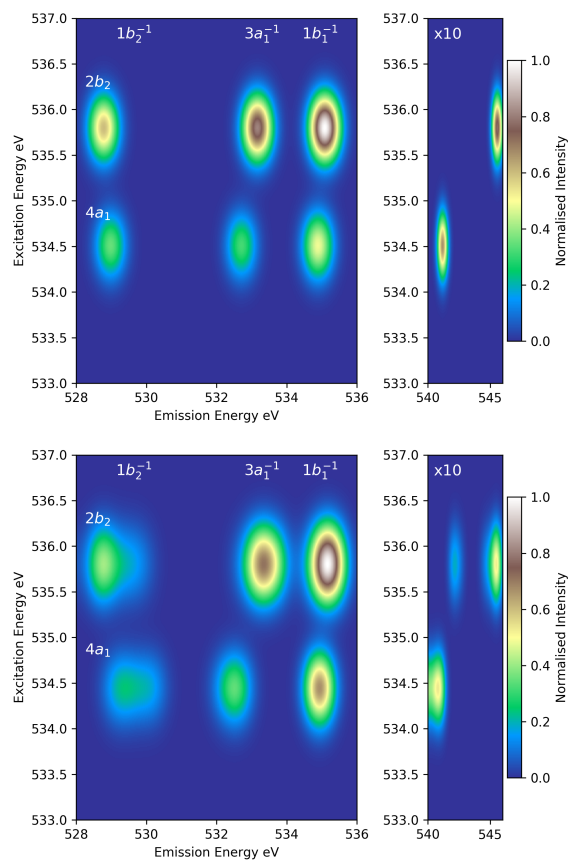


Figure 3: Simulated RIXS maps of gas phase water calculated with TDDFT methods for the equilibrium water structure (top) and sampling structures attained from AIMD simulations (bottom). Left panels shows the inelastic region (spectator emission) and the right panel shows the elastic scattering peaks (participant emission)

spectra evolve as the structure of the water molecule changes. Data is shown for the Kohn-Sham DFT calculations of the emission, but this is representative of the ADC and TDDFT calculations. A number of observations can be made. Firstly, for all states the emission energies increase as the structure changes in the core-excited state, and this effect is largest for the  $1b_2^{-1}$  state. As discussed previously, there is an important difference between the structures in the intermediate  $4a_1$  and  $2b_2$  states, where in the  $4a_1$  state one O-H bond is lengthens significantly and dissociates. The  $1b_1^{-1}$  and  $3a_1^{-1}$  emission peaks are broadened more in the  $2b_2$  state resulting in a greater spectral shift, while the  $1b_2^{-1}$  emission peak is more affected for the  $4a_1$  state.

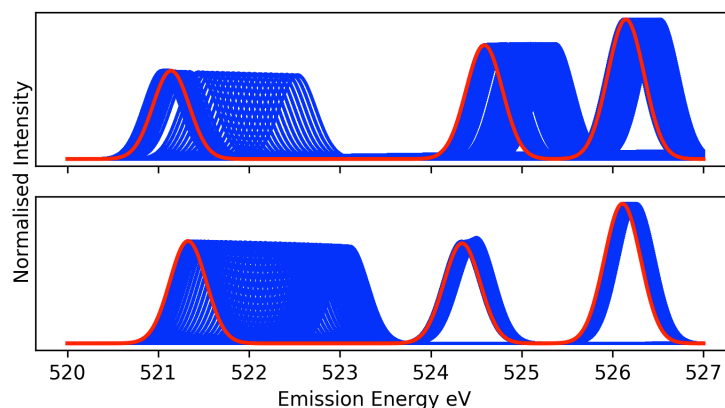


Figure 4: Resonant emission spectra for gas phase water computed using Kohn-Sham DFT (B3LYP), comparing single equilibrium conformer (red) against multiple spectra obtained from AIMD simulations (blue). Top:  $2b_2$  intermediate state, Bottom:  $4a_1$  intermediate state.

Figure 5 shows the 1-dimensional RIXS spectra for the two intermediate states along with the experimental data.<sup>8</sup> This allows a more direct comparison between the different electronic structure methods used to describe the emission. The TDDFT spectrum has been shifted by -9 eV so that it can be compared with the other methods. Initially we will discuss the  $2b_2$  state. Both Kohn-Sham DFT and TDDFT predict the energy of  $1b_1^{-1}$  line to be closer to the experimental value than ADC. However, Kohn-Sham DFT underestimates the energy separation between  $1b_1^{-1}$  and the lower energy bands, while TDDFT predicts the energy of these bands accurately. All three methods show significant broadening of the  $1b_2^{-1}$  band. For the  $4a_1$  state, experiment shows two bands for the  $1b_1^{-1}$  line. The higher energy of these corresponds to  $1b_1^{-1}$  while the lower energy

component was proposed to arise from the  $1e^{-1}$  emission of  $\text{OH}^{-}$  following dissociation. The Kohn-Sham DFT  $1b_1^{-1}$  band agrees well with experiment, but similar to the  $2b_2$  state the separation with the lower energy bands is underestimated. Both ADC and TDDFT predict the energy of the bands in quite good agreement with experiment, with the main discrepancy being the energy for  $1b_1^{-1}$  is too low. The experimental data suggests that to achieve a complete description of the  $4a_1$  state requires consideration of  $\text{OH}^{-}$ . Figure 6 shows the spectra for the three methods that include 25% of  $\text{OH}^{-}$ . This proportion of  $\text{OH}^{-}$  was chosen to achieve the correct relative heights of the two components of the  $1b_1^{-1}$  band.  $\text{OH}^{-}$  gives bands at about 526 eV ( $1e^{-1}$ ) and 522 eV ( $3a_1^{-1}$ ). A further consequence of introducing  $\text{OH}^{-}$  is that the relative intensity of the  $3a_1^{-1}$  band is reduced since  $\text{OH}^{-}$  does contribute at this energy, and this has the effect of improving the computed spectra. Overall, once a constant energy shift is applied to the emission energies, TDDFT provides an accurate description in comparison with experiment and ADC. The magnitude of this shift can be determined from comparison with  $\Delta\text{SCF}$  calculations, which means that TDDFT provides a potentially accurate approach that can be applied to study larger systems.

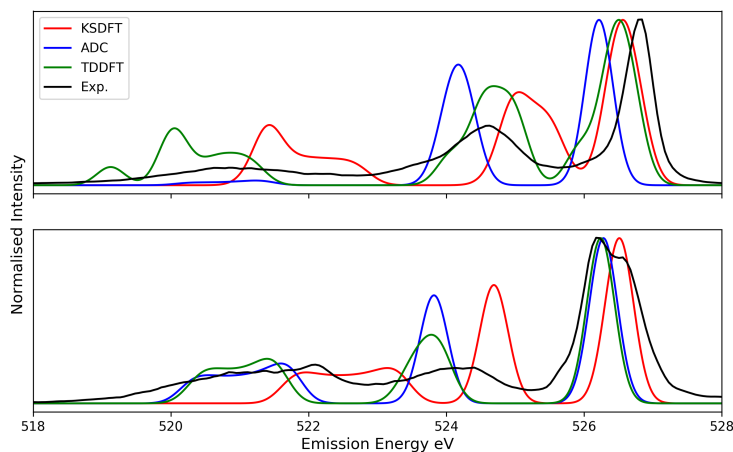


Figure 5: 1-dimensional RIXS spectra for ADC, Kohn-Sham DFT and TDDFT methods incorporating conformational sampling. Experimental data from reference 8. Top:  $2b_2$  intermediate state, Bottom:  $4a_1$  intermediate state.

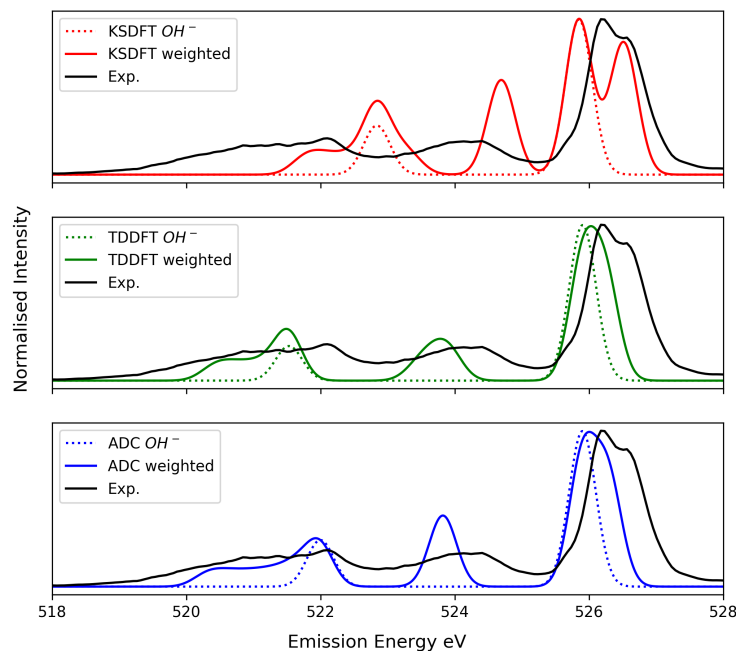


Figure 6: 1-dimensional RIXS spectra for the  $4a_1$  intermediate state computed with Kohn-Sham DFT (upper panel), TDDFT (middle panel) and ADC (lower panel) methods. Broken lines show the spectra for  $\text{OH}^-$  and the solid lines the weighted spectra for 25% of the  $\text{H}_2\text{O}$  being dissociated. Experimental data from reference 8.

## Conclusions

This study has shown how soft inelastic scattering maps can be simulated through a combination of electronic structure x-ray spectroscopy calculations and AIMD, with the RIXS intensities evaluated using the Kramers-Heisenberg formalism. Incorporating averaging over conformation, explicitly considering the core-excited intermediate state, is necessary to achieve an accurate representation of experimental data. For the water molecule, spectator shifts in the emission bands are observed and evidence of ultra-fast dynamics, particularly for the dissociative  $4a_1$  state are observed. The three approaches used to describe the emission process, namely ADC(2)-x, Kohn-Sham DFT and TDDFT with the B3LYP exchange-correlation functional all provide a similar response to the nuclear dynamics. The DFT methods are computationally less expensive and can be more readily applied to study large systems and to incorporate extensive conformational sampling. Once a

constant shift is applied to the emission energy scale, TDDFT is able to describe both inelastic and elastic scattering, while for Kohn-Sham DFT no energy shift is required but the energy of the elastic scattering bands are not predicted accurately. Furthermore, Kohn-Sham DFT tends to underestimate the energy separation between the  $1b_1^{-1}$  band and the lower energy bands. For the  $4a_1$  state good agreement with experiment can be achieved if a proportion of dissociated water molecules ( $\text{OH}^-$ ) is included. Consequently, TDDFT provides a potentially accurate approach that can be applied to study larger systems. The challenge for the methodology is the MOM procedure can fail to prevent variational collapse for high lying core-excited states and progress in this aspect is required to improve the robustness of the approach.

## Acknowledgements

This work was supported by The Leverhulme Trust under Grant [RPG-2016-103]. Steven Oatley and Pritesh Tailor are acknowledged for useful discussion regarding image processing and molecular dynamics simulations, respectively. The authors would like to thank Prof. Lothar Weinhardt (Karlsruhe Institute of Technology) for providing the experimental data.

## References

- (1) Bressler, C.; Chergui, M. Ultrafast X-ray absorption spectroscopy. *Chem. Rev.* **2004**, *104*, 1781–1812.
- (2) Nilsson, A.; Pettersson, L. Chemical bonding on surfaces probed by X-ray emission spectroscopy and density functional theory. *Surf. Sci. Rep.* **2004**, *55*, 49–167.
- (3) Chen, L. X.; Zhang, X.; Shelby, M. L. Recent advances on ultrafast X-ray spectroscopy in the chemical sciences. *Chem. Sci.* **2014**, *5*, 4136–4152.
- (4) Baker, M. L.; Mara, M. W.; Yan, J. J.; Hodgson, K. O.; Hedman, B.; Solomon, E. I. K- and L-edge X-ray absorption spectroscopy (XAS) and resonant inelastic X-ray scattering (RIXS)

- determination of differential orbital covalency (DOC) of transition metal sites. *Coord. Chem. Rev.* **2017**, *345*, 182 – 208.
- (5) Chergui, M.; Collet, E. Photoinduced structural dynamics of molecular systems mapped by time-resolved X-ray methods. *Chem. Rev.* **2017**, *117*, 11025–11065.
- (6) Ament, L. J. P.; van Veenendaal, M.; Devereaux, T. P.; Hill, J. P.; van den Brink, J. Resonant inelastic x-ray scattering studies of elementary excitations. *Rev. Mod. Phys.* **2011**, *83*, 705–767.
- (7) Weinhardt, L.; Fuchs, O.; Batchelor, D.; Bär, M.; Blum, M.; Denlinger, J. D.; Yang, W.; Schöll, A.; Reinert, F.; Umbach, E.; Heske, C. Electron-hole correlation effects in core-level spectroscopy probed by the resonant inelastic soft x-ray scattering map of C60. *J. Chem. Phys.* **2011**, *135*, 104705.
- (8) Weinhardt, L.; Benkert, A.; Meyer, F.; Blum, M.; Wilks, R. G.; Yang, W.; Bär, M.; Reinert, F.; Heske, C. Nuclear dynamics and spectator effects in resonant inelastic soft x-ray scattering of gas-phase water molecules. *J. Chem. Phys.* **2012**, *136*, 144311.
- (9) Meyer, F.; Weinhardt, L.; Blum, M.; Bär, M.; Wilks, R. G.; Yang, W.; Heske, C.; Reinert, F. Non-equivalent carbon atoms in the resonant inelastic soft X-ray scattering map of cysteine. *J. Chem. Phys.* **2013**, *138*, 034306.
- (10) Blum, M.; Odelius, M.; Weinhardt, L.; Pookpanratana, S.; Bär, M.; Zhang, Y.; Fuchs, O.; Yang, W.; Umbach, E.; Heske, C. Ultrafast proton dynamics in aqueous amino acid solutions studied by resonant inelastic soft X-ray scattering. *J. Phys. Chem. B* **2012**, *116*, 13757–13764.
- (11) Weinhardt, L.; Ertan, E.; Iannuzzi, M.; Weigand, M.; Fuchs, O.; Baer, M.; Blum, M.; Denlinger, J. D.; Yang, W.; Umbach, E.; Odelius, M.; Heske, C. Probing hydrogen bonding orbitals: resonant inelastic soft X-ray scattering of aqueous NH<sub>3</sub>. *Phys. Chem. Chem. Phys.* **2015**, *17*, 27145–27153.

- (12) Benkert, A.; Meyer, F.; Hauschild, D.; Blum, M.; Yang, W.; Wilks, R. G.; Bär, M.; Reinert, F.; Heske, C.; Weinhardt, L. Isotope effects in the resonant inelastic soft X-ray scattering maps of gas-phase methanol. *J. Phys. Chem. A* **2016**, *120*, 2260–2267.
- (13) Wernet, P.; Nordlund, D.; Bergmann, U.; Cavalleri, M.; Odelius, M.; Ogasawara, H.; Näs-lund, L. Å.; Hirsch, T. K.; Ojamäe, L.; Glatzel, P.; Pettersson, L. G. M.; Nilsson, A. The structure of the first coordination shell in liquid water. *Science* **2004**, *304*, 995–999.
- (14) Smith, J. D.; Cappa, C. D.; Messer, B. M.; Drisdell, W. S.; Cohen, R. C.; Saykally, R. J. Probing the local structure of liquid water by X-ray absorption spectroscopy. *J. Chem. Phys. B* **2006**, *110*, 20038–20045.
- (15) Fransson, T.; Harada, Y.; Kosugi, N.; Besley, N. A.; Winter, B.; Rehr, J. J.; Pettersson, L. G. M.; Nilsson, A. X-ray and electron spectroscopy of water. *Chem. Rev.* **2016**, *116*, 7551–7569.
- (16) Nilsson, A.; Pettersson, L. Perspective on the structure of liquid water. *Chem. Phys.* **2011**, *389*, 1 – 34.
- (17) Nilsson, A.; Huang, C.; Pettersson, L. G. Fluctuations in ambient water. *J. Mol. Liq.* **2012**, *176*, 2 – 16.
- (18) Nilsson, A.; Pettersson, L. G. M.; Nilsson, A. The structural origin of anomalous properties of liquid water. *Nature Commun.* **2015**, *6*, 8998.
- (19) Guo, J.-H.; Luo, Y.; Augustsson, A.; Rubensson, J.-E.; Sâthe, C.; Ågren, H.; Siegbahn, H.; Nordgren, J. X-ray emission spectroscopy of hydrogen bonding and electronic structure of liquid water. *Phys. Rev. Lett.* **2002**, *89*, 137402.
- (20) Couto, R. C.; Cruz, V. V.; Ertan, E.; Eckert, S.; Fondell, M.; Dantz, M.; Kennedy, B.; Schmitt, T.; Pietzsch, A.; Guimaraes, F. F.; Ågren, H.; Gel'mukhanov, F.; Odelius, M.; Kim-

- berg, V.; Fohlisch, A. Selective gating to vibrational modes through resonant X-ray scattering. *Nature Commun.* **2017**, *8*.
- (21) da Cruz, V. V.; Ertan, E.; Couto, R. C.; Eckert, S.; Fondell, M.; Dantz, M.; Kennedy, B.; Schmitt, T.; Pietzsch, A.; Guimaraes, F. F.; Ågren, H.; Gel'mukhanov, F.; Odelius, M.; Fohlisch, A.; Kimberg, V. A study of the water molecule using frequency control over nuclear dynamics in resonant X-ray scattering. *Phys. Chem. Chem. Phys.* **2017**, *19*, 19573–19589.
- (22) Tokushima, T.; Harada, Y.; Takahashi, O.; Senba, Y.; Ohashi, H.; Pettersson, L.; Nilsson, A.; Shin, S. High resolution X-ray emission spectroscopy of liquid water: The observation of two structural motifs. *Chem. Phys. Lett.* **2008**, *460*, 387 – 400.
- (23) Tokushima, T.; Harada, Y.; Horikawa, Y.; Takahashi, O.; Senba, Y.; Ohashi, H.; Pettersson, L. G.; Nilsson, A.; Shin, S. High resolution X-ray emission spectroscopy of water and its assignment based on two structural motifs. *J. Electron Spectrosc. Relat. Phenom.* **2010**, *177*, 192 – 205.
- (24) Guo, J.; Luo, Y. Molecular structure in water and solutions studied by photon-in/photon-out soft X-ray spectroscopy. *J. Electron Spectrosc. Relat. Phenom.* **2010**, *177*, 181–191.
- (25) Weinhardt, L.; Fuchs, O.; Blum, M.; Bär, M.; Weigand, M.; Denlinger, J.; Zubavichus, Y.; Zharnikov, M.; Grunze, M.; Heske, C.; Umbach, E. Resonant X-ray emission spectroscopy of liquid water: Novel instrumentation, high resolution, and the map approach. *J. Electron Spectrosc. Relat. Phenom.* **2010**, *177*, 206 – 211.
- (26) Tokushima, T.; Horikawa, Y.; Arai, H.; Harada, Y.; Takahashi, O.; Pettersson, L. G. M.; Nilsson, A.; Shin, S. Polarization dependent resonant x-ray emission spectroscopy of D<sub>2</sub>O and H<sub>2</sub>O water: Assignment of the local molecular orbital symmetry. *J. Chem. Phys.* **2012**, *136*, 044517.

- (27) Hunt, W. J.; Goddard, W. A. Excited States of H<sub>2</sub>O using improved virtual orbitals. *Chem. Phys. Lett.* **1969**, *3*, 414 – 418.
- (28) Ågren, H.; Carravetta, V.; Vahtras, O.; Pettersson, L. G. Direct, atomic orbital, static exchange calculations of photoabsorption spectra of large molecules and clusters. *Chem. Phys. Lett.* **1994**, *222*, 75 – 81.
- (29) Ågren, H.; Carravetta, V.; Vahtras, O.; Pettersson, L. G. M. Direct SCF direct static-exchange calculations of electronic spectra. *Theor. Chem. Acc.* **1997**, *97*, 14–40.
- (30) Triguero, L.; Pettersson, L. G. M.; Ågren, H. Calculations of near-edge x-ray-absorption spectra of gas-phase and chemisorbed molecules by means of density-functional and transition-potential theory. *Phys. Rev. B* **1998**, *58*, 8097–8110.
- (31) Shirley, E. L. Ab initio inclusion of electron-hole attraction: Application to X-ray absorption and resonant inelastic X-ray scattering. *Phys. Rev. Lett.* **1998**, *80*, 794–797.
- (32) Leetmaa, M.; Ljungberg, M.; Lyubartsev, A.; Nilsson, A.; Pettersson, L. Theoretical approximations to X-ray absorption spectroscopy of liquid water and ice. *J. Electron Spectrosc. Relat. Phenom.* **2010**, *177*, 135 – 157.
- (33) Stener, M.; Fronzoni, G.; de Simone, M. Time dependent density functional theory of core electrons excitations. *Chem. Phys. Lett.* **2003**, *373*, 115 – 123.
- (34) Tsuchimochi, T.; Kobayashi, M.; Nakata, A.; Imamura, Y.; Nakai, H. Application of the Sakurai-Sugiura projection method to core-excited-state calculation by time-dependent density functional theory. *J. Comp. Chem.* **2008**, *29*, 2311–2316.
- (35) Ekström, U.; Norman, P. X-ray absorption spectra from the resonant-convergent first-order polarization propagator approach. *Phys. Rev. A* **2006**, *74*, 042722.
- (36) Ekström, U.; Norman, P.; Carravetta, V.; Ågren, H. Polarization propagator for X-ray spectra. *Phys. Rev. Lett.* **2006**, *97*, 143001.

- (37) Besley, N. A.; Asmuruf, F. A. Time-dependent density functional theory calculations of the spectroscopy of core electrons. *Phys. Chem. Chem. Phys.* **2010**, *12*, 12024–12039.
- (38) Capano, G.; Penfold, T.; Besley, N.; Milne, C.; Reinhard, M.; Rittmann-Frank, H.; Glatzel, P.; Abela, R.; Rothlisberger, U.; Chergui, M.; Tavernelli, I. The role of Hartree-Fock exchange in the simulation of X-ray absorption spectra: A study of photoexcited  $[\text{Fe}(\text{bpy})_3]^{2+}$ . *Chem. Phys. Lett.* **2013**, *580*, 179 – 184.
- (39) Besley, N. A. Fast time-dependent density functional theory calculations of the x-ray absorption spectroscopy of large systems. *J. Chem. Theory Comput.* **2016**, *12*, 5018–5025.
- (40) Asmuruf, F. A.; Besley, N. A. Calculation of near-edge X-ray absorption fine structure with the CIS(D) method. *Chem. Phys. Lett.* **2008**, *463*, 267 – 271.
- (41) Wenzel, J.; Wormit, M.; Dreuw, A. Calculating core-level excitations and x-ray absorption spectra of medium-sized closed-shell molecules with the algebraic-diagrammatic construction scheme for the polarization propagator. *J. Comp. Chem.* **2014**, *35*, 1900–1915.
- (42) Wenzel, J.; Wormit, M.; Dreuw, A. Calculating X-ray absorption spectra of open-shell molecules with the unrestricted algebraic-diagrammatic construction scheme for the polarization propagator. *J. Chem. Theory Comput.* **2014**, *10*, 4583–4598.
- (43) Wenzel, J.; Holzer, A.; Wormit, M.; Dreuw, A. Analysis and comparison of CVS-ADC approaches up to third order for the calculation of core-excited states. *J. Chem. Phys.* **2015**, *142*, 214104.
- (44) Besley, N. A. Equation of motion coupled cluster theory calculations of the X-ray emission spectroscopy of water. *Chem. Phys. Lett.* **2012**, *542*, 42 – 46.
- (45) Wadey, J. D.; Besley, N. A. Quantum chemical calculations of X-ray emission spectroscopy. *J. Chem. Theory Comput.* **2014**, *10*, 4557–4564.

- (46) Zhang, Y.; Mukamel, S.; Khalil, M.; Govind, N. Simulating valence-to-core X-ray emission spectroscopy of transition metal complexes with time-dependent density functional theory. *J. Chem. Theory Comp.* **2015**, *11*, 5804–5809.
- (47) Roper, I. P.; Besley, N. A. The effect of basis set and exchange-correlation functional on time-dependent density functional theory calculations within the Tamm-Dancoff approximation of the x-ray emission spectroscopy of transition metal complexes. *J. Chem. Phys.* **2016**, *144*, 114104.
- (48) Zhovtobriukh, I.; Besley, N. A.; Fransson, T.; Nilsson, A.; Pettersson, L. G. M. Relationship between x-ray emission and absorption spectroscopy and the local H-bond environment in water. *J. Chem. Phys.* **2018**, *148*, 144507.
- (49) Hanson-Heine, M. W.; George, M. W.; Besley, N. A. Kohn-Sham density functional theory calculations of non-resonant and resonant x-ray emission spectroscopy. *J. Chem. Phys.* **2017**, *146*, 094106.
- (50) Hanson-Heine, M. W.; George, M. W.; Besley, N. A. Density functional theory calculations of the non-resonant and resonant X-ray emission spectroscopy of carbon fullerenes and nanotubes. *Chem. Phys. Lett.* **2018**, *696*, 119 – 124.
- (51) Kramers, H. A.; Heisenberg, W. Über die streuung von strahlung durch atome. *Zeitschrift für Physik A Hadrons and Nuclei* **1925**, *31*, 681–708.
- (52) Gel'mukhanov, F.; Ågren, H. Resonant inelastic x-ray scattering with symmetry-selective excitation. *Phys. Rev. A* **1994**, *49*, 4378–4389.
- (53) Luo, Y.; Agren, H.; Gel'mukhanov, F. Symmetry assignments of occupied and unoccupied molecular orbitals through spectra of polarized resonance inelastic x-ray scattering. *J. Phys. B-At. Mol. Opt.* **1994**, *27*, 4169.

- (54) Luo, Y.; Ågren, H.; Gel'mukhanov, F. Polarization anisotropy in resonant x-ray emission from molecules. *Phys. Rev. A* **1996**, *53*, 1340.
- (55) Gel'mukhanov, F.; Ågren, H. Resonant X-ray Raman scattering. *Physics Reports* **1999**, *312*, 87–330.
- (56) Kashtanov, S.; Augustsson, A.; Luo, Y.; Guo, J.-H.; Sâthe, C.; Rubensson, J.-E.; Siegbahn, H.; Nordgren, J.; Ågren, H. Local structures of liquid water studied by x-ray emission spectroscopy. *Phy. Rev. B* **2004**, *69*, 024201.
- (57) Gel'Mukhanov, F. K.; Mazalov, L.; Kondratenko, A. A theory of vibrational structure in the X-ray spectra of molecules. *Chem. Phys. Lett.* **1977**, *46*, 133–137.
- (58) Ljungberg, M. P.; Pettersson, L. G.; Nilsson, A. Vibrational interference effects in x-ray emission of a model water dimer: Implications for the interpretation of the liquid spectrum. *J. Chem. Phys.* **2011**, *134*, 044513.
- (59) Nilsson, A.; Tokushima, T.; Horikawa, Y.; Harada, Y.; Ljungberg, M. P.; Shin, S.; Pettersson, L. G. Resonant inelastic X-ray scattering of liquid water. *J. Electron Spectrosc. Relat. Phenom.* **2013**, *188*, 84–100.
- (60) Schirmer, J.; Trofimov, A. Intermediate state representation approach to physical properties of electronically excited molecules. *J. Chem. Phys.* **2004**, *120*, 11449–11464.
- (61) Wormit, M.; Rehn, D. R.; Harbach, P. H.; Wenzel, J.; Krauter, C. M.; Epifanovsky, E.; Dreuw, A. Investigating excited electronic states using the algebraic diagrammatic construction (ADC) approach of the polarisation propagator. *Mol. Phys.* **2014**, *112*, 774–784.
- (62) Rehn, D. R.; Dreuw, A.; Norman, P. Resonant Inelastic X-ray Scattering Amplitudes and Cross Sections in the Algebraic Diagrammatic Construction/Intermediate State Representation (ADC/ISR) Approach. *J. Chem. Theory Comput.* **2017**, *13*, 5552–5559.

- (63) Ljungberg, M. P.; Nilsson, A.; Pettersson, L. G. Semiclassical description of nuclear dynamics in x-ray emission of water. *Phys. Rev. B* **2010**, *82*, 245115.
- (64) Ljungberg, M.; Zhovtobriukh, I.; Takahashi, O.; Pettersson, L. G. Core-hole-induced dynamical effects in the x-ray emission spectrum of liquid methanol. *J. Chem. Phys.* **2017**, *146*, 134506.
- (65) Takahashi, O.; Ljungberg, M. P.; Pettersson, L. G. X-ray Emission Spectrum of Liquid Ethanol: Origin of Split Peaks. *J. Phys. Chem. B* **2017**, *121*, 11163–11168.
- (66) Ljungberg, M. P. Vibrational effects in x-ray absorption and resonant inelastic x-ray scattering using a semiclassical scheme. *Phys. Rev. B* **2017**, *96*, 214302.
- (67) Uejio, J. S.; Schwartz, C. P.; Saykally, R. J.; Prendergast, D. Effects of vibrational motion on core-level spectra of prototype organic molecules. *Chem. Phys. Lett.* **2008**, *467*, 195 – 199.
- (68) Fouda, A. E. A.; Besley, N. A. Assessment of basis sets for density functional theory-based calculations of core-electron spectroscopies. *Theor. Chem. Acc.* **2017**, *137*, 6.
- (69) Besley, N. A.; Gilbert, A. T. B.; Gill, P. M. W. Self-consistent-field calculations of core excited states. *J. Chem. Phys.* **2009**, *130*, 124308.
- (70) Tolbatov, I.; Chipman, D. M. Benchmarking density functionals and Gaussian basis sets for calculation of core-electron binding energies in amino acids. *Theor. Chem. Acc.* **2017**, *136*, 82.
- (71) Wenzel, J.; Dreuw, A. Physical properties, exciton analysis, and visualization of core-excited states: An intermediate state representation approach. *J. Chem. Theory Comput.* **2016**, *12*, 1314–1330.
- (72) Neville, S. P.; Averbukh, V.; Ruberti, M.; Yun, R.; Patchkovskii, S.; Chergui, M.; Stolow, A.; Schuurman, M. S. Excited state X-ray absorption spectroscopy: Probing both electronic and structural dynamics. *J. Chem. Phys.* **2016**, *145*, 144307.

- (73) Hirata, S.; Head-Gordon, M. Time-dependent density functional theory within the Tamm–Dancoff approximation. *Chem. Phys. Lett.* **1999**, *314*, 291–299.
- (74) Besley, N. A.; Peach, M. J. G.; Tozer, D. J. Time-dependent density functional theory calculations of near-edge X-ray absorption fine structure with short-range corrected functionals. *Phys. Chem. Chem. Phys.* **2009**, *11*, 10350–10358.
- (75) Robinson, D.; Besley, N. A. Modelling the spectroscopy and dynamics of plastocyanin. *Phys. Chem. Chem. Phys.* **2010**, *12*, 9667–9676.
- (76) Buckley, M. W.; Besley, N. A. A theoretical study of the near edge X-ray absorption fine structure of amino acids and proteins. *Chem. Phys. Lett.* **2011**, *501*, 540 – 546.
- (77) Fogarty, R. M.; Matthews, R. P.; Clough, M. T.; Ashworth, C. R.; Brandt-Talbot, A.; Corbett, P. J.; Palgrave, R. G.; Bourne, R. A.; Chamberlain, T. W.; Vander Hoogerstraete, T.; Thompson, P. B. J.; Hunt, P. A.; Besley, N. A.; Lovelock, K. R. J. NEXAFS spectroscopy of ionic liquids: experiments versus calculations. *Phys. Chem. Chem. Phys.* **2017**, *19*, 31156–31167.
- (78) Shao, Y. et al. Advances in molecular quantum chemistry contained in the Q-Chem 4 program package. *Mol. Phys.* **2015**, *113*, 184–215.
- (79) Takahashi, O.; Pettersson, L. G. Functional dependence of core-excitation energies. *J. Chem. Phys.* **2004**, *121*, 10339–10345.
- (80) Vinson, J.; Jach, T.; Müller, M.; Unterumsberger, R.; Beckhoff, B. Quasiparticle lifetime broadening in resonant x-ray scattering of  $\text{NH}_4\text{NO}_3$ . *Phys. Rev. B* **2016**, *94*, 035163.
- (81) Ågren, H.; Cesar, A.; Carravetta, V. On the constant resonance width approximation for core electron ionization. *Chem. Phys. Lett.* **1987**, *139*, 145 – 148.
- (82) Ågren, H.; Luo, Y.; Gel'mukhanov, F.; Jensen, H. J. A. Screening in resonant x-ray emission of molecules. *J. Electron Spectrosc. Relat. Phenom.* **1996**, *82*, 125–134.

- (83) Laksman, J.; Månsson, E. P.; Sankari, A.; Céolin, D.; Gisselbrecht, M.; Sorensen, S. L. Rapid bond rearrangement in core-excited molecular water. *Phys. Chem. Chem. Phys.* **2013**, *15*, 19322–19329.
- (84) Hjelte, I.; Piancastelli, M.; Fink, R.; Bjärneholm, O.; Bässler, M.; Feifel, R.; Giertz, A.; Wang, H.; Wiesner, K.; Ausmees, A.; Miron, C.; Sorensen, S.; Svensson, S. Evidence for ultra-fast dissociation of molecular water from resonant Auger spectroscopy. *Chem. Phys. Lett.* **2001**, *334*, 151 – 158.
- (85) Ye, H.-Z.; Welborn, M.; Ricke, N. D.; Voorhis, T. V.  $\sigma$ -SCF: A direct energy-targeting method to mean-field excited states. *J. Chem. Phys.* **2017**, *147*, 214104.
- (86) Schirmer, J.; Trofimov, A.; Randall, K.; Feldhaus, J.; Bradshaw, A.; Ma, Y.; Chen, C.; Sette, F. K-shell excitation of the water, ammonia, and methane molecules using high-resolution photoabsorption spectroscopy. *Phys. Rev. A* **1993**, *47*, 1136.
- (87) Fouda, A.; Ryde, U. Does the DFT self-interaction error affect energies calculated in proteins with large QM systems? *J. Chem. Theory Comput.* **2016**, *12*, 5667–5679.
- (88) Takahashi, O.; Odelius, M.; Nordlund, D.; Nilsson, A.; Bluhm, H.; Pettersson, L. G. Auger decay calculations with core-hole excited-state molecular-dynamics simulations of water. *J. Chem. Phys.* **2006**, *124*, 064307.
- (89) Richings, G.; Polyak, I.; Spinlove, K.; Worth, G.; Burghardt, I.; Lasorne, B. Quantum dynamics simulations using Gaussian wavepackets: the vMCG method. *Int. Rev. Phys. Chem.* **2015**, *34*, 269–308.